Digital Object Identifier: https://doi.org/10.1109/JPHOTOV.2020.3012631

Optimization of Back Contact Grid Size in Al_2O_3-Rear-Passivated Ultrathin CIGS PV Cells by 2-D Simulations

Jackson Lontchi , Maria Zhukova , Milan Kovacic , Janez Krc, Wei-Chao Chen , Marika Edoff , Sourav Bose , Pedro M. P. Salomé , Julie Goffard, Andrea Cattoni, L. Gouillart, Stephane Collin , Viktoria Gusak, and Denis Flandre

***Abstract*—We present a simulation strategy using ATLAS-2D to optimize the back-contact hole grid (i.e., size and pitch of openings) of the Al_2O_3-rear-passivation layer in ultrathin Cu(In,Ga)Se_2 photovoltaic cells. We first discuss and compare our simulation model with a series of experimental nonpassivated and passivated cells to decouple the crucial passivation parameters. The simulation results follow the experimental trends, highlighting the beneficial effects of the passivation on the cell performances. Furthermore, it stresses the influence of the passivation quality at the Al_2O_3/Cu(In,Ga)Se_2 (CIGS) interface and of the contact resistance at the Mo/CIGS interface within the openings. Further simulations quantify significant improvements in short-circuit current and open-circuit voltage for different sizes of openings in the Al_2O_3 layer, relative to an excellent passivation quality (i.e., high density of negative charges in the passivation layer). However, a degradation is predicted for a poor passivation (i.e., low density of such charges) or a high contact resistance. Consequently, we point out an optimum in efficiency when varying the opening widths at fixed hole-pitch and fixed contact resistance. At equivalent contact resistance, simulations predict that the sizes of the pitch and openings can be increased without optimal performance losses when maintaining a width to pitch ratio around 0.2. This simulation trends have been confirmed by a series of experiments, indicating that it is crucial to care about the dimensions of the opening grid and the contact resistance of passivated cells. These simulation results provide significant insights for optimal cell design and characterizations of passivated UT-CIGS PV cells.**

***Index Terms*—2-D modeling, Al_2O_3 passivation, electrical characterization, opening/pitch, ultrathin Cu(In,Ga)Se_2 (CIGS PV) cells.**

This work was supported by the ARCIGS-M project within the EU H2020 research and innovation program under Grant 720887. *(Corresponding author: Jackson Lontchi.)*

Jackson Lontchi, Maria Zhukova, and Denis Flandre are with the ICTEAM Institute, Université catholique de Louvain, 1348 Louvain-la-Neuve, Belgium (e-mail: jackson.lontchi@uclouvain.be; maria.zhukova@uclouvain.be; denis.flandre@uclouvain.be).

Milan Kovacic and Janez Krc are with the Faculty of Electrical Engineering, University of Ljubljana, 1000 Ljubljana, Slovenia (e-mail: milan.kovacic@fe.uni-lj.si; janez.krc@fe.uni-lj.si).

Wei-Chao Chen and Marika Edoff are with the Ångström Laboratory, Department of Engineering Sciences, Uppsala University, 751 21 Uppsala, Sweden (e-mail: chen.weichao@angstrom.uu.se; marika.edoff@angstrom.uu.se).

Sourav Bose and Pedro M. P. Salomé are with the International Iberian Nanotechnology Laboratory, 4715-330 Braga, Portugal (e-mail: sourav.bose@inl.int; pedro.salome@inl.int).

Julie Goffard, Andrea Cattoni, L. Gouillart, and Stephane Collin are with the Centre for Nanoscience and Nanotechnology, University Paris-Sud/Paris-Saclay, 91120 Palaiseau, France (e-mail: j.goffard@outlook.fr; andrea.cattoni@c2n.upsaclay.fr; stephane.collin@c2n.upsaclay.fr).

Viktoria Gusak is with Solibro Research AB, 75651 Uppsala, Sweden (e-mail: viktoria.gusak@gmail.com).

I. Introduction

NOWADAYS, ultrathin (UT) Cu(In,Ga)Se_2 (CIGS) technology is widely investigated for low-cost fabrication, low material usage and for flexible photovoltaic (PV) and building integrated photovoltaic applications [1], [2]. However, lowering the thickness of the absorber layer below the standard micrometer scale reduces light absorption and reveals degradation mechanisms that limit the PV performances of the cell [3], [4]. Therefore, engineering ultrathin cells require high-precision optimization methods to improve the performances to the level of the standard thicker cells.

Many research works have proposed different optimization approaches to increase the performances of UT-CIGS PV cells. The group at Uppsala University has reported on several experiments with grading of the CIGS absorber layer by different [Ga]/([In]+[Ga]) ratios [5]–[8]. They reported the beneficial effect of the Ga-grading on a 0.5 μm thick CIGS cell with an improvement in absolute value of efficiency (Eff) around 2.5% due to an increase of the open-circuit voltage (V_{oc}) and fill-factor (FF) values [5] with the possibility to engineer the bandgap by means of evaporation profile variations [6]. In collaboration with the Uppsala group, Kotipalli *et al.* in UCLouvain have reported a decrease of deep defects near the space charge region which was found to be beneficial for improving the V_{oc} [9]. Several works reported the passivation of the Mo/CIGS interface by the introduction of a very thin oxide layer [10]–[17]. The main effect is the reduction of the rear recombination of photogenerated carriers that leads to an increase of the short-circuit current (J_{sc}) and the V_{oc} especially for ultrathin cells [18], [19]. Another largely investigated approach is the intentional introduction of alkali elements to improve the transport properties and the resulted performance of thin CIGS PV cells [20], [21]. Moreover, to compensate the decrease of the absorption due to thickness reduction of the CIGS layer, researchers proposed

the introduction of a rear optical reflector materials to reflect the nonabsorbed incident light back into the CIGS to improve J_{sc} [22]–[26]. Other solutions to decrease optical losses include improving front transparent contacts, usage of anti-reflection structures, introduction of textures, among others [27]. Implementing different approaches to achieve high performance requires high-level engineering, a significant amount of time, and expensive experiments. Therefore, simulations are helpful to reproduce, as accurately as possible, the experimental cell structures and measurement results by implementing different parameters and different designs. Several papers have been already reported on simulations of thin and UT-CIGS PV cells with significant results on the effects of various properties on the cell performances [28]–[32]. Vermang *et al.* reported on Al_2O_3 rear-passivated thick CIGS cell with nano-sized local rear point contacts [11] that show a significant improvement in V_{oc} compared with reference (i.e., nonpassivated) cells. However, the influence of the fixed charge density at the rear passivation layer along with the dimensions of the rear contact holes (i.e., size and pitch of opening grid) and the effect of the contact resistance have not yet been investigated in UT-CIGS PV cells.

In this article, we present a 2-D model of reference and Al_2O_3-rear-passivated UT-CIGS cells built with ATLAS-2D simulation tool. We first discuss and compare the general trends of simulation results with the experimental cell results in the dark and their correlations with the PV parameters under illumination. Next, we discuss the concurrent influence of the passivation quality and of the contact resistance on the performance of the passivated cells for different opening sizes. The last section deals with the optimization of the opening width to pitch ratio in the passivated layer using the full 2-D model simulation results, compared with experiments.

A final aim of the study is to show that a suitable 2-D modeling can help to understand the performances of the Al_2O_3-rear-passivated UT-CIGS cells with regards to the size of the back-contact grid; furthermore, how it can provide useful predictions, trends and directions for their optimal design and accurate characterization, as well as to revisit apparent contradictory results sometimes observed in experiments.

II. Study Details

A. Modeling Details

The modeling methodology has been built at Université catholique de Louvain (UCLouvain) with the contribution of several partners collaborating within ARCIGS-M. 2-D simulations were performed using Silvaco ATLAS 2D with Deckbuild 4.6.2.R interface under room temperature, the dark and AM1.5 illumination conditions. The global model structure used for ATLAS 2D simulations of UT-CIGS solar cells is presented in Fig. 1 and consists of a p-type CIGS layer of 500 nm thickness as absorber, an n-type CdS of 50 nm thickness as buffer layer, 100 nm of i-ZnO, and 300 nm of Al-doped ZnO as transparent conductive oxide layers. Molybdenum (Mo) and aluminum (Al)/nickel (Ni) were used as rear and front contact electrodes, respectively. A 25 nm thin layer of Al_2O_3 with openings has been introduced at the Mo/CIGS interface as passivation layer

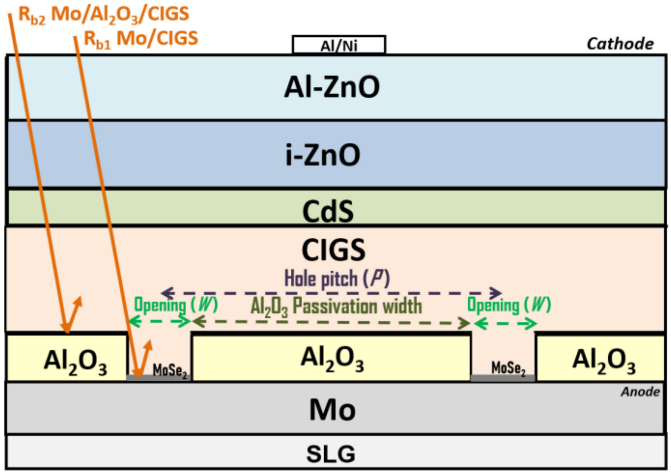

Fig. 1. ATLAS 2D ARCIGS-M structure model of Al_2O_3-rear-passivated UT-CIGS cell showing rear-openings width (W) and hole pitch (P) including back reflection coefficients (R_{b1}, R_{b2}).

containing a negative fixed charge density (Q_f) in cm^{-2} and an interface traps density (D_{it}) in cm^{-2}/eV.

The total width of the passivated structure model (see Fig. 1) is 1.1 μm corresponding to 2 times the pitch of 500 nm and 2 times an initial contact hole of 50 nm.

To approach the experiment as accurately as possible, the electrical properties of the $MoSe_2$ layer, formed during the CIGS process, were considered at the (Mo,$MoSe_2$)/CIGS interfaces (see Fig. 1). A work function value of 5.65 eV was used for (Mo,$MoSe_2$), forming an ohmic contact with CIGS [33], whereas 4.9 eV was used for Mo at Mo/Al_2O_3/CIGS interface [34]. For simplification, we will mention Mo/CIGS instead of (Mo,$MoSe_2$)/CIGS for the rest of the text. The work function value of 4.7 eV was used at the front Al/Ni alloy front metal according to literature [35].

Beside electrical parameters integrated in ATLAS, an external optical semi-coherent model was used with the Sun*Shine* simulation tool by Ljubljana University to support accurate determination of realistic optical properties of UT-CIGS PV cell [36]. This provided some optical parameters to embed in ATLAS model such as back reflectance coefficients (R_{b1}, R_{b2}) corresponding to the optical reflection coefficients at the rear Al_2O_3 interface (R_{b2}) or back Mo contact (R_{b1}) into the CIGS (see Fig. 1). These constant average values were determined iteratively, by matching the absorptance curves of the CIGS layer obtained with detailed simulations of the entire cell structure using wavelength-dependent reflectance spectra and simplified simulations using an average R_b value. Values of 20% and 45% have been obtained for R_{b1} and R_{b2}, respectively, in agreement with [22]. Other optical parameters such as complex refractive n, k indices of included layers have been provided from optical simulations and literature [36], [37] in order to genuinely represent light behavior in the model. The baseline parameters of our model are presented in Table I.

The key material parameters of the passivation layers in this model are the negative charge density (Q_f) and the interface

TABLE I
BASELINE PARAMETERS OF THE MODEL

	CIGS	CdS	i:ZnO	Al:ZnO
d (nm)	500	50	100	300
E_g (eV)	1.15	2.4	3.3	3.3
χ (eV)	4.5	4.45	4.55	4.55
ε_r	13.6	10	9	9
N_c (cm^{-3})	3.1×10^{18}	1.3×10^{18}	3.1×10^{18}	3.1×10^{18}
N_v (cm^{-3})	1.8×10^{19}	9.1×10^{18}	1.8×10^{19}	1.8×10^{19}
V_e (cm/s)	3.9×10^{7}	3.1×10^{7}	2.4×10^{7}	2.4×10^{7}
V_h (cm/s)	1.4×10^{7}	1.6×10^{7}	1.3×10^{7}	1.3×10^{7}
μ_e (cm^2/Vs)	100	72	100	100
μ_h (cm^2/Vs)	12.5	20	31	3
N_A (cm^{-3})	3.0×10^{16}	5.0×10^{17}	1.0×10^{17}	5.0×10^{18}
Bulk defect parameters [32]				
N_t (cm^{-3})	1.0×10^{14}	1.0×10^{16}	1.0×10^{16}	1.0×10^{16}
σ_e (cm^2)	1.0×10^{-15}	1.0×10^{-15}	1.0×10^{-15}	1.0×10^{-15}
σ_h (cm^2)	1.0×10^{-11}	1.0×10^{-13}	5.0×10^{-13}	5.0×10^{-13}
	Rear contact		Front contact	
W_f (eV)	4.9 (Mo); 5.65 ($MoSe_2$)		4.7 (Al/Ni)	
SRV (cm/s)	10^7 (Ref.); 10^2 (Pass.)		10^7	
R (Ω·cm^2)	R_s, R_c variables; R_{sh} not implemented			

E_g = band gap energy, ε_r = relative permittivity, d = layer thickness, χ = affinity; μ_e, μ_h = electron and hole mobility, V_e, V_h = velocity of electrons and holes, N_c, N_v = effective density of states in conduction and valence bands, N_A = Doping density, N_t = total density of defects, σ_e, σ_h = capture cross-section of electrons and holes, W_f = work function, R = resistance.

trap density ($D_{\rm it}$). The Q_f density defines the amount of fixed negative charge introduced by the Al_2O_3 passivation layer at the interface which, in turn, influences the electron and hole densities at the rear Mo/CIGS interface by electric field effect; they are implemented in the model as negative values where the sign represents the type of charges. $D_{\rm it}$ defines the amount of electrons/holes traps at the interface that recombines the photogenerated carriers. As usual in these models, Q_f is expressed per unit area of the interface (cm^{-2}), while $D_{\rm it}$ is expressed per unit area of the interface and per unit of energy level in the semiconductor bandgap (cm^{-2}·eV^{-1}).

Previous experiments estimated the absolute value of Q_f density at the Al_2O_3/CIGS passivated interface in the range of 10^{12} cm^{-2} and the $D_{\rm it}$ in the range of 10^{11} cm^{-2}·eV^{-1} [10], [32]. The effect of the $D_{\rm it}$ is introduced in this model through the surface velocity recombination (SRV) according to the following formula [38]:

$$\mathrm{SRV} = \frac{U_s}{\Delta n} \quad \text{with} : U_{\rm S} \cong \frac{\left(n_{\rm s}p_{\rm s} - n_i^2\right) * q^{-1} v_{\rm th} D_{\rm it}}{\frac{n_{\rm s}}{\sigma p} + \frac{p_{\rm s}}{\sigma n}} \qquad (1)$$

where n_s and p_s are the surface densities of electrons and holes, respectively, σ_n, σ_p are the cross-sections of electrons and holes, respectively, $v_{\rm th}$ being the thermal velocity, $U_{\rm S}$ is the recombination rate, and Δn is the excess carrier density. The used SRV value will be discussed below.

This model intrinsically simulates the behavior of the cell assuming an infinite shunt resistance ($R_{\rm sh}$) with no additional external series resistance ($R_{\rm s}$). However, a specific contact resistance ρ_c in Ω·cm^2 (noted R_c in this article) can be specified at the Metal/Semiconductor interface. Divided by the contact area, it yields a full series resistance, noted R_c when normalized to 1 cm^2. We use it here to directly emulate the experimental $R_{\rm s}$ for reference cells, whereas for passivated cells, we convert $R_{\rm s}$ in an equivalent R_c at the Mo/CIGS interface within the contact holes according to the following equation:

$$R_C = R_s * \frac{W}{P}. \qquad (2)$$

The reason for this approximation is that, for the reference cell, the Mo/CIGS interface covers the whole cell area, whereas for the passivated cells, that contact interface appears only within the openings that cover a *W/P* ratio of the total cell area. The experimental $R_{\rm s}$ value then leads to an approximated contact resistance R_c at the Mo/CIGS rear interface that represents the losses due to series resistance depending on the opening size. Such approach limits the approximation related to the 2-D modelling compared with the 3-D reality and reproduces the experimental trends as demonstrated in the next section.

B. Experimental Details

The first experimental cells used in this work have been realized by different research groups within the European H2020 ARCIGS-M project. They consist of a series of reference and Al_2O_3-rear-passivated UT-CIGS cell with 500 nm CIGS thickness fabricated on soda lime glass (SLG) substrates at the International Iberian Nanotechnology Laboratory (INL).

Reference cells consist of SLG/Mo/500 nm–CIGS/50 nm–CdS/100 nm-i:ZnO/300 nm-Al:ZnO with Ni/Al/Ni as front contact. For passivated cells, a 25 nm thin layer of Al_2O_3 has been deposited on top of Mo before the CIGS deposition. A grid of contact holes has been opened within the Al_2O_3 layer with a diameter (W = 200 nm) and an equidistant hole pitch (P = 2 μm). Details about fabrication process can be found at the reference [39].

Another series of reference and Al_2O_3-rear-passivated UT-CIGS cells with different hole pitches have been fabricated on SLG substrates at the Centre for Nanoscience and Nanotechnology (CNRS) with the collaboration of Solibro Research AB (Solibro). The structure of the reference cell is the same as in the previous series from INL (SLG/Mo/CIGS/CdS/i:ZnO/Al:ZnO/(Ni/Al/Ni)), whereas the Al_2O_3 layer in passivated cells has various contact hole patterns. The diameter of the openings has been kept constant (W = 300 nm) but the distance between the centers of two adjacent holes (pitch) has been varied from 1 to 4 μm. The aim was to investigate the effects of the contact grid dimensions on the cell performances compared with simulation predictions. Results of characterizations for this series of experiments are presented and compared with simulation results in regards to the variation of the width and pitch of openings.

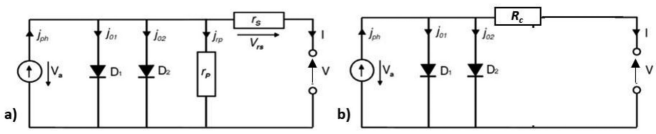

Fig. 2. (a) Equivalent electrical circuit for the two-diode model of a PV cell, (b) Reduced model for ATLAS simulations with the contact resistance.

C. Electrical Characterization Details

The experimental cells were characterized by current density–voltage (*J–V*) measurements in the dark conditions and under illumination. The dark *J–V* measurements were performed at UCLouvain with the PM8PS probe station in the four wires configuration at room temperature, whereas the PV parameters were extracted from the *J–V* curves under AM1.5 illumination conditions at each fabrication partner site. In order to understand the obtained PV performances, a special attention has been paid to the precise analysis of the dark *J–V* characteristic for the different cells from experiments and simulations.

The analytical two-diode model of a PV cell was used to extract the electrical parameters of experimental devices from the *J–V* curves in the dark. Fig. 2 shows the equivalent electrical circuit for the two-diode model of a PV cell [see Fig. 2(a)] and the reduced model developed in this study with ATLAS without shunt resistance [see Fig. 2(b)] but with contact resistance used to emulate the series resistance.

Diode 1 (D_1) represents the diffusion current related to the main PN junction and is characterized by its current density J_{01} and its nonideality factor n_1. Diode 2 (D_2) represents the generation/recombination (*G/R*) current and is characterized by its current density J_{02} and its nonideality factor n_2.

The full characteristic equation of the two-diode model under illumination is presented as follows:

$$J(V) = J_{\mathrm{PH}} - J_{01}\left[\exp\left(\frac{q(V+R_sJ)}{n_1kT}\right)-1\right] - J_{02}\left[\exp\left(\frac{q(V+R_sJ)}{n_2kT}\right)-1\right] - \frac{V+R_{\mathrm{s}}J}{R_{\mathrm{sh}}} \quad (3)$$

where V is the applied voltage, J is the measured output current density, J_{PH} is the incident photocurrent density, q is the charge of the electron, k is the Boltzmann constant, and T is the temperature.

In this model, each diode is analyzed at corresponding bias regions to discriminate the different contributions to the total current density. The *G/R* and the diffusion currents in CIGS PV cells may not be initially considered as completely separated since the nonideality factors are indeed quite different from those ideally found in silicon cells. Nevertheless, their different contributions to the total dark current of the cell can be clearly distinguished in the *J–V* curves; while, when varying the simulation parameters, the simulations confirm the dominance of G*/R* phenomena (D_2) in reverse and low-voltage forward operation or of the diffusion (D_1) at higher voltage in forward conditions. The last term in (1) represents the shunt leakage current density (J_{sh}) investigated in reverse bias region [40]. It is obvious, but worth reminding, that one should be careful about the appropriate range of voltage selected for the determination of J_{02} to discriminate the effect of the shunt. It is recommended to extract R_{sh} at the minimum of *dJ/dV* to avoid underestimating J_{02} as discussed in [41].

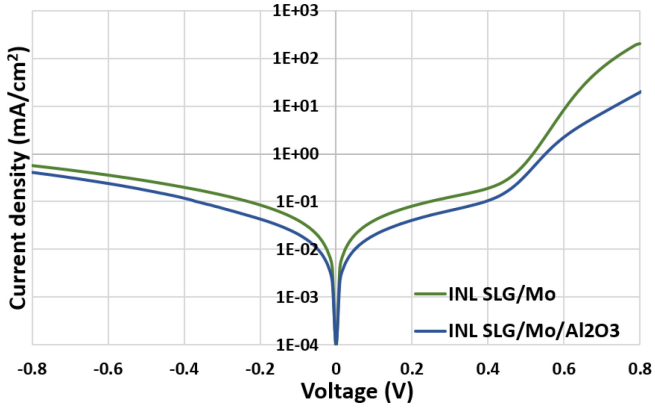

Fig. 3. Dark *J–V* curves in logarithm scale for INL reference (SLG/Mo) and Al_2O_3-rear-passivated (SLG/Mo/Al_2O_3) UT-CIGS cells. The width to pitch ratio (W/P) for the passivated cell in this simulation is 0.1. The reference device (SLG/Mo) shows higher current density values for all voltage values indicating a worse electrical behavior than the passivated device (SLG/Mo/Al_2O_3).

This methodology has been applied for the determination of the dark electrical parameters of the experimental cells in this study. This is highly necessary in this work due to the ATLAS limitation (i.e., no R_{sh}). With this approach, our modeling results fit the experimental trends rather well and are coherent with the PV parameters extracted under illumination as discussed hereafter.

III. Results and Discussions

A. Characterizations Versus Simulations: Effects of Al_2O_3-Rear-Passivation on UT-CIGS Cells

In this section, based on the series of experimental cells from INL compared with simulations, we present and discuss the effects of the passivation on the *J–V* characteristic in the dark and their correlations with the PV parameters obtained under illumination. Next, the obtained results are compared with simulation results for different parameters of the passivation layer. Fig. 3 presents the *J–V* curves of reference and passivated cells measured in the dark at room temperature. The electrical parameters measured in the dark from Fig. 3 and the PV parameters measured under illumination are listed in Table II [39].

We observe in Fig. 3 that the *G/R* current density J_{02} as well as the diffusion current density J_{01} in the dark is reduced for the passivated cell compared with the reference, meaning a decrease of the diffusion and a decrease of the *G/R* phenomenon due to the introduction of the passivation layer. The decrease of the recombination results in a better collection of the photo-generated electron/hole pairs under illumination that leads to an increase of the J_{sc}, while a decrease of the diffusion current leads to better transport properties at the main CIGS/CdS junction that improves the V_{oc} value above the reference one. Thanks to the Al_2O_3-rear-passivation, in this experiment, an increase in

TABLE II
ELECTRICAL PARAMETERS FOR INL REFERENCE AND PASSIVATED UT-CIGS CELLS MEASURED IN THE DARK AND UNDER ILLUMINATION

Electrical parameters	SLG/Mo	SLG/Mo/Al_2O_3
Measured in the dark		
J_{01} (mA/cm^2)	7.13×10^{-5}	4.20×10^{-5}
J_{02} (mA/cm^2)	2.06×10^{-2}	6.68×10^{-3}
n_1	1.51	2.12
n_2	3.19	3.22
R_s ($\Omega\cdot$cm^2)	0.69	1.84
R_{sh} ($\Omega\cdot$cm^2)	2.11×10^{3}	3.86×10^{3}
Measured under illumination		
J_{sc} (mA/cm^2)	21.40	24.30
V_{oc} (mV)	573.10	609.10
FF (%)	66.50	64.70
Eff (%)	8.15	9.50

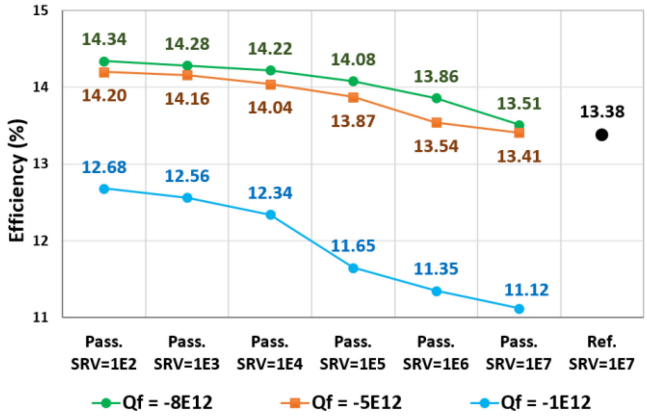

Fig. 4. Efficiency of reference cell with SRV $= 1 \times 10^7$ cm/s and passivated cells with different SRV values from 1×10^7 to 1×10^2 cm/s and different Q_f densities (-8×10^{12} cm^{-2}, -5×10^{12} cm^{-2}, -1×10^{12} cm^{-2}). The passivated cells with the highest Q_f density show better efficiency above the reference for each SRV value indicating the importance of the negative oxide charges to improve the cell performances.

absolute value of J_{sc} by about 2.88 mA/cm^2 and an increase in absolute value of V_{oc} by 36 mV is observed. We observed a reduction of the FF for passivated compared with reference due to an increase of the series resistance compensated by the increase of the product $J_{sc}*V_{oc}$ that leads to an increase of absolute value of the Eff by 1.4%.

This series of experiments have been reproduced by simulation with our model for different properties of the Al_2O_3 passivation layer on UT-CIGS PV cells. The opening width W was kept constant at 200 nm for a 2 μm pitch like in the experiment. Our approximation model of resistances described in Section II-C has been applied to the experimental resistance values that gives an R_c of 0.69 $\Omega\cdot$cm^2 for the reference cell (Ref.) and 0.18 $\Omega\cdot$cm^2 (i.e., 1.81∗0.2/2) for the passivated cell (Pass.), respectively. In experiments, according to the Q_f density introduced by the oxide layer at the Al_2O_3/CIGS interface, the passivation mechanism reduces the recombination by attracting holes at the oxide/semiconductor interface and repelling electrons. This electrical field has a significant impact on cell performance, as shown in Fig. 4, where we clearly see the effect of the recombination velocity as well as of Q_f on the efficiency.

The Mo/CIGS SRV value has been varied from 10^2 to 10^7 cm/s for three specific Q_f values (-8×10^{12} cm^{-2}, -5×10^{12} cm^{-2}, and -1×10^{12} cm^{-2}) chosen in the range of experimental values [10]. The SRV value of 10^7 cm/s was maintained at the Mo/CIGS interface.

It is important to highlight that experimentally, Q_f, D_{it}, and SRV are not independent parameters as the amount of Q_f and D_{it} will define the effective experimental SRV value. However, as experimentally one can introduce passivation layers with different properties that are not easy to untangle, in simulation we use these parameters independently. Moreover, Fig. 4 decouples the influences of the Q_f and the SRV with regards to the efficiency.

For each value of simulated SRV, as thus, of D_{it}, passivated cells with the highest Q_f density always provides for the highest cell performance, demonstrating that a large value of negative

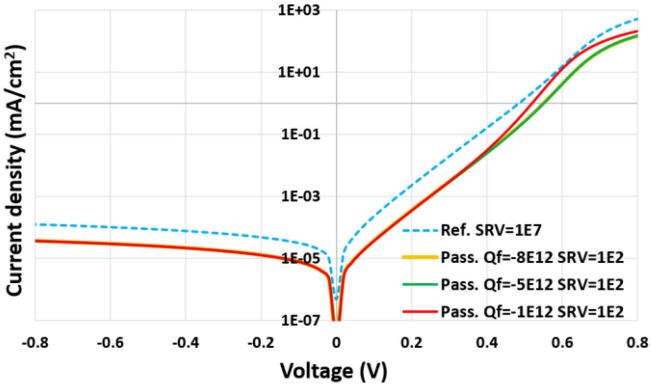

Fig. 5. Simulated J–V curves in the dark for reference cells (blue dashes) with an SRV of 1×10^7 cm.s^{-1} and passivated cells with an SRV of 1×10^2 cm/s with three different Q_f values of -8×10^{12} cm^{-2} (yellow lines), -5×10^{12} cm^{-2} (green lines), and -1×10^{12} cm^{-2} (red lines). The yellow line is overlapped with the green one. Simulation reproduces the trends of the experiment showing the effect of the Q_f density on the electrical performances of the cell.

Q_f is more important and efficient with regards to electrical field passivation, than a reduction of D_{it} or SRV (hence improving chemical passivation), in agreement with studies in other materials [42], [43].

We plotted in Fig. 5 the J–V curves in the dark resulting from the simulation of the passivated cells with the three different Q_f values for the SRV of 1×10^2 cm/s compared with the reference cell; the electrical parameters simulated in the dark (J_{01}, J_{02}, n_1, and n_2) as well as the PV parameters simulated under illumination are summarized in Table III. Note that the S-shape observed in experimental INL dark J–V curves (see Fig. 3) is the influence of low shunt resistance; its degradation effect on the PV performances under illumination, especially on the FF, is observed for very low shunt resistance value only (below 1×10^3 $\Omega\cdot$cm^2). Our simulated J–V curves do not account for that as our model miss the contribution of the shunt resistance.

TABLE III
ELECTRICAL PARAMETERS SIMULATED IN THE DARK AND UNDER ILLUMINATION FOR REFERENCE AND PASSIVATED CELLS WITH THREE DIFFERENT Q_f

Electrical parameters	Ref.	Pass. Q_f=-8×10^{12}	Pass. Q_f=-5×10^{12}	Pass. Q_f=-1×10^{12}
Simulated in the dark				
J_{01} (mA/cm^2)	5.50×10^{-6}	4.90×10^{-7}	4.59×10^{-7}	2.01×10^{-6}
J_{02} (mA/cm^2)	2.14×10^{-5}	3.70×10^{-6}	3.70×10^{-6}	3.68×10^{-6}
n_1	1.57	1.46	1.45	1.50
n_2	1.69	1.72	1.72	1.72
Simulated under illumination				
J_{sc} (mA/cm^2)	26.62	28.13	28.04	26.79
V_{oc} (mV)	659.79	700.74	695.05	661.58
FF (%)	76.15	72.75	72.87	71.54
Eff (%)	13.38	14.34	14.20	12.68

We observe in Fig. 5 that, when the absolute value of the Q_f density is high enough (–5 × 10^{12} cm^{-2} or –8 × 10^{12} cm^{-2}), the dark current density is reduced both in forward and reverse operations (see values in Table III) as observed experimentally. The reduction of the dark current in reverse and at low voltage (leakage current) induces a reduction of the J_{02} current density related to the recombination phenomena, this contributes to the improvement of the J_{sc} of about 1.4–1.5 mA/cm^2 in Table III. The reduction of the diffusion current density in the dark J_{01} linked to the main junction is related to the passivation-induced rear electrical field and induces an improvement of the V_{oc}, here about 40 mV. The link between the J_{01} and the V_{oc} can be approximated by the following first-order well-known formula [44]:

$$V_{oc} = \frac{nkT}{q} \ln\left[\frac{J_{Ph}}{J_0} + 1\right] \quad (4)$$

where *n* is the nonideality factor, *k* is the Boltzmann constant, *q* is the charge of the electron, J_{Ph} is the photocurrent generated by incident light, and J_0 is the diffusion current density of the cell.

Reducing the absolute value of Q_f of the passivated cell from 8 × 10^{12} cm^{-2} to 5 × 10^{12} cm^{-2} leads to a slight increase of the dark current, especially visible at high voltage around J_{01} that causes a slight reduction of the V_{oc} and the J_{sc} under illumination (by about 5 mV and 0.1 mA/cm^2) while they still remain significantly above the reference performances.

When the absolute value of Q_f of the passivated cell is reduced down to 1 × 10^{12} cm^{-2}, a significant increase of the diffusion current is observed that reduces the V_{oc} according to (4). Our simulation results show that to the first order, it is related to an inversion of the electrical field at the rear interface of the passivated CIGS cells. The *G/R* forward and reverse current densities show a slight increase that supposes an increase of the recombination which reduces the J_{sc} close to the reference. We notice a significant decrease of the *FF* that reduces the efficiency of the cell below the reference one. The increase of the diffusion current in the dark is surprising as it worsens the device performance even though the Al_2O_3 layer is introduced to passivate the rear Mo/CIGS interface. Particularly, its detrimental effect on the J_{01} of the main junction, when the Q_f density is very low was not reported or investigated before.

This simulation results could help to understand some experimental results where the cell performances are either improved or reduced after Al_2O_3-rear-passivation. This latest can be attributed to a poor passivation quality, or to a high contact resistance in other cases as will be discussed in the next section. Therefore, an increase of the diffusion current J_{01} in the dark and a low V_{oc} under illumination, respectively, from one passivated cell to another, can be used to characterize poor passivation (i.e., insufficiently negative Q_f) experimentally. Further investigations are ongoing to better understand these intricate effects of the Al_2O_3-rear-passivation layer especially on UT-CIGS solar cells. However, our simulations predict an improvement in absolute values of J_{sc} and V_{oc} of 1.51 mA/cm^2 and 41 mV, respectively, thanks only to the passivation with a Q_f of –8 × 10^{12} cm^{-2} and an SRV value of 1 × 10^2 cm/s. These gains are close to the ones obtained in experiments and the differences may come from variations of material properties.

B. *Optimization of Opening Width of the Al_2O_3 Layer*

While in our previous study we demonstrated that the simulations fit well the experimental results, we have not changed the patterning configuration. The geometry, the size, and the distribution of the contact holes have been found to be important for the performance of the passivated cells. In this section, we quantify the impact of pattern dimensions in terms of the trends that their variations induce on the PV parameters of passivated cells compared with reference ones. Gains on PV-parameters (ΔJ_{sc}, ΔV_{oc}, ΔFF, and ΔEff) are reported as the difference between the absolute value of a parameter after passivation and the one obtained for a reference cell. Therefore, a gain equal to 0 corresponds to a case equal to the reference cell in terms of performance. We present in Fig. 6 the gains on the four PV parameters for a passivated cell with different opening width (*W*) at a fixed pitch ($P = 0.5$ μm) with ($R_c = 0.1$ Ω·cm^2) and without contact resistance ($R_c = 0$ Ω·cm^2) at the Mo/CIGS interface within the openings. Moreover, we considered for this simulation, passivated cells with the two specific Q_f values –8 × 10^{12} cm^{-2} and –1 × 10^{12} cm^{-2} at the Al_2O_3/CIGS interface for a fixed SRV of 1 × 10^2 cm/s.

We observe that, when the negative Q_f density is high enough (8 × 10^{12} cm^{-2}), the J_{sc} of the passivated cells are improved compared with reference as discussed before. However, we find that its value decreases when increasing the opening width values. We can attribute this decrease of J_{sc} to the increase of the effective recombination rate at the Mo/CIGS interface that increases when increasing the openings and thereby the contact area. V_{oc} follows the same trend and its values are higher than the reference only for a certain range of opening width, where the passivation area is large compared with the contact hole area and the gains are limited by the value of the contact resistance. With R_c taken into consideration (green curve in Fig. 6), the fill-factor

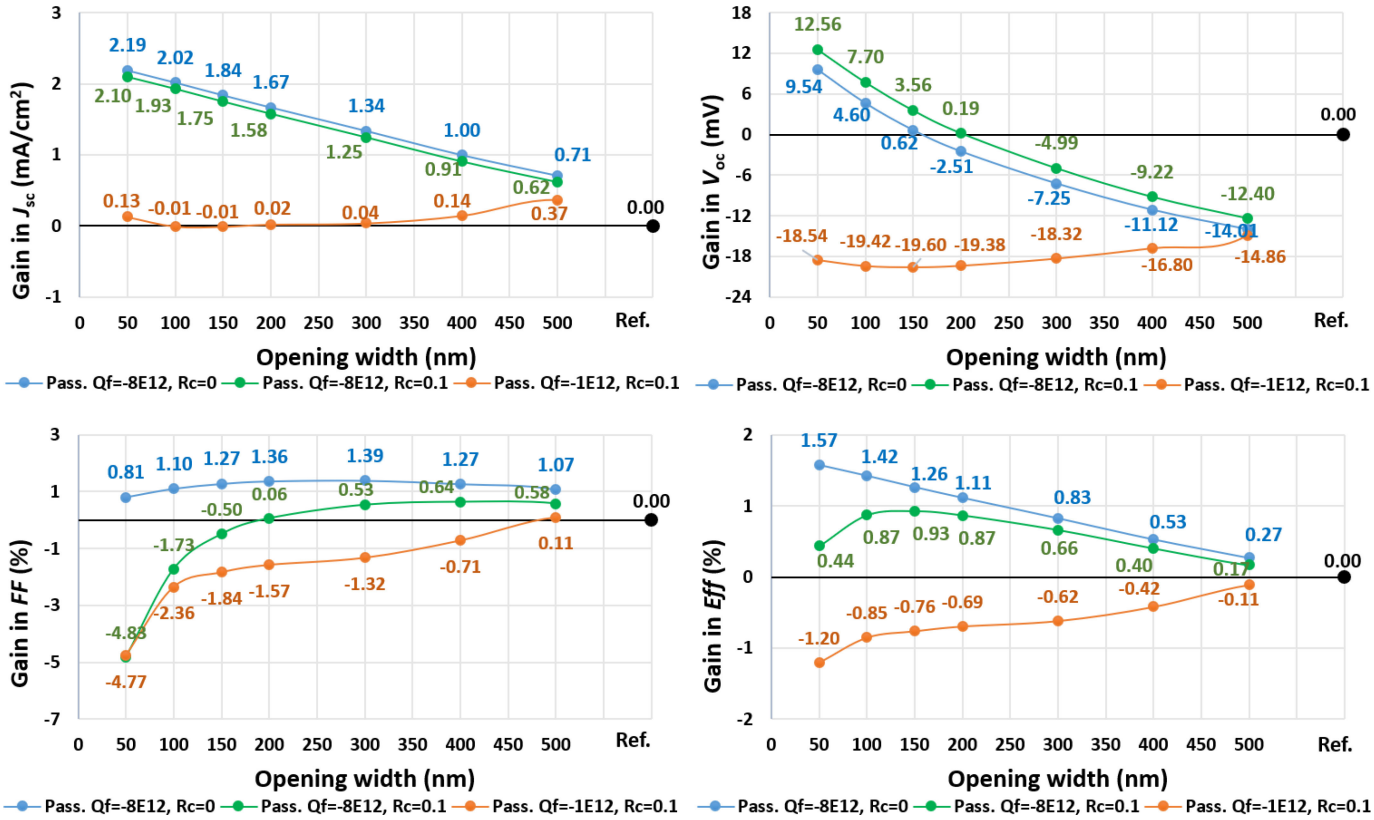

Fig. 6. Gains on absolute values of PV-parameters for passivated UT-CIGS cells for different opening widths at fixed pitch of 0.5 μm with and without R_c and for two Q_f densities: $Q_f = -8 \times 10^{12}$ cm^{-2} with $R_c = 0\ \Omega{\cdot}$cm^2 (blue curves), $Q_f = -8 \times 10^{12}$ cm^{-2} with $R_c = 0.1\ \Omega{\cdot}$cm^2 (green curves), and $Q_f = -1 \times 10^{12}$ cm^{-2} with $R_c = 0.1\ \Omega{\cdot}$cm^2 (red curves). The results show several dependencies highlighting that several parameters enter into play when defining the best pattern of the rear passivation.

is degraded below the reference for low opening widths because of an increase of the series resistance already predicted by simulations and observed experimentally. However, when the contact hole area becomes larger compared with the passivation area, the FF of the passivated cell is improved compared with reference.

The resulting efficiency of the cell, which is a combination of the aforementioned parameters, first increases from small openings, where passivation has a higher effect on the performances, passes by an optimum value and then decreases when the size of openings are further increased due to the reduction of the passivation area that leads to an increase of the recombination at the Mo/CIGS interface.

All those trends and positive effects of passivation are negated when the absolute value of Q_f is reduced down to 1×10^{12} cm^{-2}. Simulations show that, in this case, electrons present at the Al_2O_3/CIGS interface recombine with photogenerated holes, degrading the PV parameters of the cells, finally leading to worse performance than the reference cell. This is an important result as it demonstrates the ultimate importance of having negative Q_f values.

We point out here the presence of an optimum in efficiency for passivated cells at an opening width in the range 100–150 nm for a fixed hole pitch of 0.5 μm that correspond to an opening width to pitch ratio between 0.2 and 0.3 and the sensitivity of the performance to a variation of the opening width around that optimum, for nonzero contact resistance. This can help to explain the small differences of performances observed for different cells on a same sample or from one process to another, due to variation of W, Q_f, and R_c, apart from other material and defect state differences. This novel result about optimal *W/P* ratio shows the crucial importance to have and to control a suitable design of the contact openings as well as a lower contact resistance for best performances in Al_2O_3-rear-passivated UT-CIGS cells.

C. Optimization of Hole Pitch Sizes

In this section, we extended the study to different pitch distances to clear out a general trend on the optimal configuration with regards to W and P. The aim was to investigate the possibility to increase the size of the openings and the pitch to make it less challenging during fabrication of the rear contact grid. We simulated the passivated cell for different opening widths and different pitches. We increased the openings width from 100 to 3000 nm considering different pitches P from 1 to 4 μm with typical density of negative charges $Q_f = -8 \times 10^{12}$ cm^2 and $R_c = 0.1\ \Omega{\cdot}$cm^2. The impact on the PV performances has been simulated and compared with reference cells. Simulation results, summarized in Fig. 7, show the different gains in J_{sc}, V_{oc}, FF,

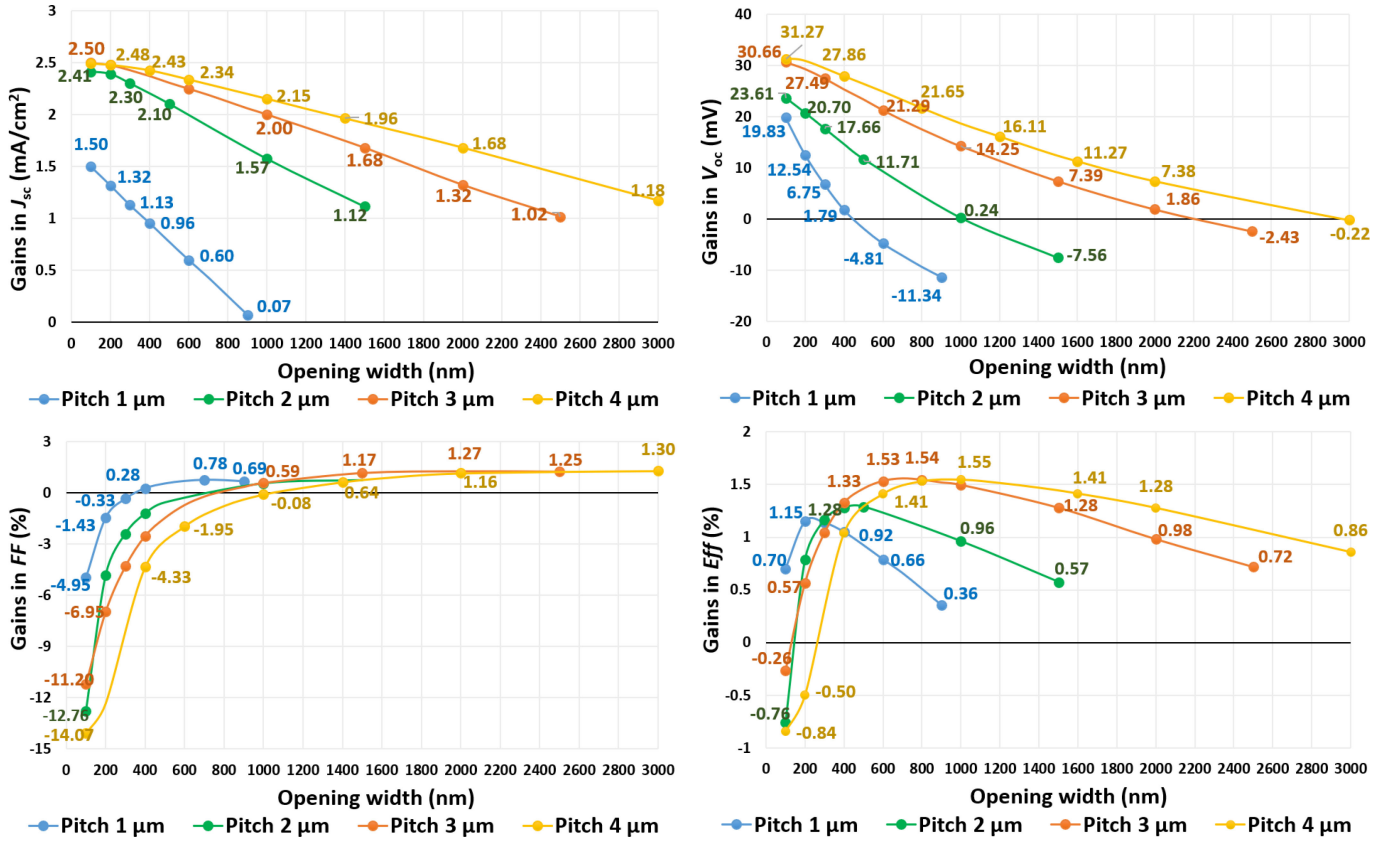

Fig. 7. Gains on absolute values of PV-parameters for passivated cells compared with reference for hole pitches of 1 μm (blue curve), 2 μm (green curve), 3 μm (orange curve), and 4 μm (yellow curve) as a function of different opening widths at fixed R_c and fixed Q_f of -8×10^{12} cm^2. The optimum shifts to the right and increases when increasing the pitch, showing possibilities for optimization of the rear contact pattern.

and Eff compared with reference versus opening widths for each pitch size.

At constant W, we observe an increase of the gains ΔJ_{sc} and ΔV_{oc} that tend to saturate at high pitches for small openings, when we increase the pitch and therefore the passivated area. On the other hand, the gain ΔFF decreases at constant W as we reduce the opening width to pitch ratio (W/P) and increase the series resistance implemented as contact resistance in this study. As a result, the optimum gain in efficiency ΔEff, when the material parameters and the specific contact resistance are kept constant, increases toward larger W for larger P values. For example, increasing the pitch up to 2–4 μm is not detrimental for the cell performances compared with a cell with 1 μm pitch as long as we increase the optimum W up to 400–800 nm. This result is very important for the cell design and provides direction toward next processes as experimentally, a large opening grid is less difficult and less costly to produce.

We predict in this study an increase of the efficiency by about 1.4%–1.5% in absolute value, thanks to passivation which agrees closely to the gains generally demonstrated by experiments with an opening to pitch (W/P) ratio around 0.2 for each cell configuration that is close to our model test structure. However, during the fabrication processes, many phenomena can occur leading to a variation of material and interface/bulk defect properties in the cells. These different possible variations can induce either a positive or a negative effect on the PV performances of the cell.

It should be noted that two different trends are observed and explained on the two sides of the optimum predicted by this study for W/P ratios of about 0.2: 1) for W/P ratios $>$ 0.4–0.5, a loss of V_{oc} can be observed when compared with the reference, though the rear interface is well passivated and the J_{sc} is higher as well as the efficiency, or 2) for $W/P < 0.1$, large gains in J_{sc} and in V_{oc} are negated in terms of efficiency by a large loss on FF due to the high series resistance.

The series of reference and Al_2O_3-rear-passivated cells from CNRS and Solibro with different hole pitches at fixed opening width will serve as experimental study case. The values of hole pitches for the passivated cells are $P = 1$, 2, 3, and 4 μm with an average measured opening width W of 300 nm. The cells have been characterized under AM1.5 illumination and the measured average PV parameters as well as the average series and shunt resistances of all devices per sample types are summarized in Table IV.

We observe that, thanks to the passivation, both the J_{sc} and the V_{oc} of the passivated cells are higher than the reference, with gains of about 1.5 to 2.8 mA/cm^2 and 12 to 19 mV, respectively. On the contrary, the FF values of passivated cells are strongly degraded, as expected from the higher series resistance induced by localized contacts through small holes. Depending on the

TABLE IV
AVERAGE EXPERIMENTAL PV-PARAMETERS AND RESISTANCES OF REFERENCE AND PASSIVATED CELLS MEASURED UNDER ILLUMINATION FROM CRNS/SOLIBRO SERIES WITH DIFFERENT PITCH SIZES ($P = 1$, 2, 3, AND 4 μm) AT CONSTANT OPENING ($W = 300$ nm)

	Ref.	Pass.			
Pitch *(μm)*	-	1	2	3	4
W/P ratio	-	0.3	0.15	0.1	0.08
R_s ($\Omega\cdot$cm^2)	0.13	1.94	0.4	1.69	2.53
R_{sh} ($\Omega\cdot$cm^2)	455.2	473.4	365.42	547.95	831.95
J_{sc} (mA/cm^2)	20.02	21.56	22.85	21.45	22.05
V_{oc} (mV)	663.5	682	677.6	681.7	676.1
FF (%)	71.85	64.69	67.85	58.29	61.11
Eff (%)	10.94	10.34	11.48	9.26	9.81

different dimensions of the opening grid (*W/P* ratio) and the resistance values, the efficiencies of passivated cells are either improved or reduced as compared with the reference cell when increasing P from 1 to 4 μm, with a best efficiency achieved for a pitch $P = 2$ μm. The latter case that corresponds to a *W/P* ratio of 0.15 agrees with simulation predictions of the optimum around 0.2. When increasing the pitch, the *W/P* ratio decreases and the gains in J_{sc} and in V_{oc} are negated by the large loss on FF due to resistances as predicted by simulations. These results are close to our simulation trends but show some variations in performance between the real devices and the theoretical simulation models probably due to fabrication processes variabilities.

It has to be noted that in real cells, the back-grid openings are organized in a very regular matrix in all directions. Therefore, a series of regular openings in the third direction will then behave like a line contact with a different series resistance and passivation area than the 2-D model that assumes homogeneous properties in the third dimension. However, as we fit the empirical contact resistance R_c in the 2-D model from the experimental R_s value and the opening width to pitch ratio, the specific R_c value obtained in a 3-D model would be different, but the equivalent R_s would be the same. With regards to the effect of the passivation area, it should be noted that what matters is the lateral collection of photogenerated carriers which depends on the diffusion length compared with the distance to the contact. In a regular 3-D model, in the worst case, that distance can only become 40% larger than the half-pitch considered in the 2-D model. That could probably result in different absolute values for optimal W and P parameters, but the general trends should remain the same and keep the message of this work, i.e., that the optimal *W/P* is around 0.15–0.20, supported by both simulations and experiments. For example, Sozzi in [45] reported on a 3-D simulation work, an optimal opening width of 400 nm for a 2 μm pitch and R_c of 10^{-4} $\Omega\cdot$cm^2 for absolute value of (negative) $Q_f \geq 5 \times 10^{12}$ cm^{-2} on a 3 μm CIGS PV cell that fit with our results ($W/P = 0.2$). However, compared with their work, our simulations have targeted ultrathin CIGS cells, discussed in-depth the effects of the passivation properties on the dark current and on the different PV parameters under illumination, and furthermore achieved an optimization of the full back grid (W and P) dimensions supported by experimental results.

IV. CONCLUSION

The key of success of the proposed modeling of the rear contact grid in passivated UT-CIGS cells is the correlation of the general trends with the experimental results while limited for the absolute values by the exact material properties especially the bulk and interface defect states and the resistances definition. We discussed the optimization of the Al_2O_3-rear-passivated cell according to the dimensions of the contact openings in the passivation layer and its influence on the electrical behavior in the dark current and on the PV-parameters of the cell under illumination. The latter mostly depends on passivation quality (i.e., density of negative fixed oxide charges) and contact resistance. It comes out that apart from the improvement due to the material qualities, especially for the oxide passivation layer, it is crucial to optimize the dimensions of the openings to improve the transport with less resistance effects, i.e., keep a good *FF*, while maintaining excellent rear passivation. Experimental results sometimes show different, even opposed, or detrimental effects of rear passivation on cell performances under illumination. Our simulations relate these contradictory observations to the interplay between the area and quality of the passivation layer on one hand and the size, density, and contact resistance of openings in this passivation layer on the other hand. Variations of these parameters around their optimum values can lead to positive or negative trends on the cell performances. Subsequently, characterizing these performances under illumination is not sufficient to assess the passivation quality due to the possible impact of the shunt and series resistances. Our extensive results demonstrate that the quality of the passivation can be directly related to increases of J_{sc} under illumination and reduction of diffusion (J_{01}) and G/R (J_{02}) diode currents in the dark when compared with the unpassivated cells, both experimentally and by simulations. On the other hand, V_{oc} under illumination is not a straightforward indicator of the quality of the passivation interface since it may become higher or smaller than the reference cell depending on the opening width to pitch ratio and not on the quality of the passivation layer. This study revealed the presence of an optimum in PV performances for an opening width to pitch (*W/P*) ratio around 0.2 for a good passivation quality. We finally show how a suitable 2-D modeling can yield additional and more accurate insights on the results of characterizations of cells and hence can guide the experiences and provide useful interpretation, direction, and trends for the fabrication process.

REFERENCES

[1] J. Ramanujam and U. P. Singh, "Copper Indium gallium selenide based solar cells - A review," *Energy Environ. Sci.*, vol. 10, pp. 1306–1319, 2017.

[2] B. P. Jelle, "Building integrated photovoltaics: A concise description of the current state of the art and possible research pathways," *Energies*, vol. 9, 2016, Art. no. 21.

[3] J. Goffard *et al.*, "Nanostructured back mirror for ultra-thin CIGS solar cells," in *Proc. 31th Eur. Photovolt. Sol. Energy Conf.*, pp. 1050–1052, 2015.

[4] N. Naghavi *et al.*, "Ultrathin Cu(In,Ga)Se_2 based solar cells," *Thin Solid Films*, vol. 633, pp. 55–60, 2017.

[5] O. Lundberg, M. Edoff, and L. Stolt, "The effect of Ga-grading in CIGS thin film solar cells," *Thin Solid Films*, vol. 480–481, pp. 520–525, 2005.

[6] S. Schleussner, U. Zimmermann, T. Wätjen, K. Leifer, and M. Edoff, "Effect of gallium grading in Cu(In,Ga)Se_2 solar-cell absorbers produced by multi-stage co-evaporation," *Sol. Energy Mater. Sol. Cells*, vol. 95, pp. 721–726, 2011.

[7] M. Edoff, S. Schleussner, E. Wallin, and O. Lundberg, "Technological and economical aspects on the influence of reduced Cu(In,Ga)Se_2 thickness and Ga grading for co-evaporated Cu(In,Ga)Se_2 modules," *Thin Solid Films*, vol. 519, pp. 7530–7533, 2011.

[8] W.-C. Chen, L. Stolt, and M. Edoff, "Ga/(Ga + In) grading effects on ultra-thin (UT) CIGS solar cell," in *Proc. IEEE Photovolt. Spec. Conf.*, Jun. 2019.

[9] R. Kotipalli *et al.*, "Influence of Ga/(Ga + In) grading on deep-defect states of Cu(In,Ga)Se_2 solar cells," *Phys. Status Solidi RRL*, vol. 9, pp. 157–160, 2015.

[10] R. Kotipalli *et al.*, "Investigating the electronic properties of Al_2O_3/Cu(In, Ga)Se2 interface," *AIP Adv.*, vol. 5, 2015, Art. no. 107101.

[11] B. Vermang, V. Fjällström, J. Pettersson, P. Salomé, and M. Edoff, "Development of rear surface passivated Cu(In,Ga)Se_2 thin film solar cells with nano-sized local rear point contacts," *Sol. Energy Mater. Sol. Cells*, vol. 117, pp. 505–511, 2013.

[12] B. Vermang, F. Rostvall, V. Fjällström, and M. Edoff, "Potential-induced optimization of ultra-thin rear surface passivated CIGS solar cells," *Phys. Status Solidi RRL*, vol. 8, 2014, Art. no. 908.

[13] J. M. V. Cunha, C. Rocha, C. Vinhais, P. A. Fernandes, and P. M. P. Salomé, "Understanding the AC equivalent circuit response of ultrathin Cu(In,Ga)Se_2 solar cells," *IEEE J. Photovolt.*, vol. 9, no. 5, pp. 1442–1448, Sep. 2019.

[14] S. Bose *et al.*, "Optical lithography patterning of SiO_2 layers for interface passivation of thin film solar cells," *Sol. RRL*, vol. 2, 2018, Art. no. 1800212.

[15] J. M. V. Cunha *et al.*, "Insulator materials for interface passivation of Cu(In,Ga)Se_2 thin films," *IEEE J. Photovolt.*, vol. 8, no. 5, pp. 1313–1319, Sep. 2018.

[16] D. Ledinek, P. M. P. Salomé, C. Hägglund, U. Zimmermann, and M. Edoff, "Rear contact passivation for high bandgap Cu(In, Ga)Se_2 solar cells with a flat Ga profile," *IEEE J. Photovolt.*, vol. 8, no. 3, pp. 864–870, May 2018.

[17] P. M. P. Salomé *et al.*, "Passivation of interfaces in thin film solar cells: Understanding the effects of a nanostructured rear point contact layer," *Adv. Mater. Interfaces*, vol. 5, no. 2, 2018, Art. no. 1701101.

[18] B. Vermang, V. Fjällström, X. Gao, and M. Edoff, "Improved rear surface passivation of Cu(In,Ga)Se_2 solar cells: A combination of an Al_2O_3 rear surface passivation layer and nanosized local rear point contacts," *IEEE J. Photovolt.*, vol. 4, no. 1, pp. 486–492, Jan. 2014.

[19] B. Vermang *et al.*, "Highly reflective rear surface passivation design for ultra-thin Cu(In,Ga)Se_2 solar cells," *Thin Solid Films*, vol. 582, pp. 300–303, 2015.

[20] F. Werner *et al.*, Alkali treatments of Cu(In,Ga)Se_2 thin-film absorbers and their impact on transport barriers," *Prog. Photovolt. Res. Appl.*, vol. 26, pp. 911–923, 2018.

[21] Y. Sun *et al.*, "Review on alkali element doping in Cu(In,Ga)Se_2 thin films and solar cells," *Engineering*, vol. 3, pp. 452–459, 2017.

[22] J. Goffard *et al.*, "Light trapping in ultrathin CIGS solar cells with nanostructured back mirrors," *IEEE J. Photovolt.*, vol. 7, no. 5, pp. 1433–1441, Sep. 2017

[23] L. Gouillart *et al.*, "Development of reflective back contacts for high-efficiency ultrathin Cu(In,Ga)Se_2 solar cells," *Thin Solid Films*, vol. 672, pp. 1–6, 2019.

[24] O. Poncelet *et al.*, "Optimization of rear reflectance in ultra-thin CIGS solar cells towards >20% efficiency," *Sol. Energy*, vol. 146, pp. 443–452, 2017.

[25] T. S. Lopes *et al.*, "Rear optical reflection and passivation using a nanopatterned metal/dielectric structure in thin-film solar cells," *IEEE J. Photovolt.*, vol. 9, no. 5, pp. 1421–1427, Sep. 2019.

[26] J. M. V. Cunha *et al.*, "Decoupling of optical and electrical properties of rear contact cigs solar cells," *IEEE J. Photovolt.*, vol. 9, no. 6, pp. 1857–1862, Nov. 2019.

[27] M. Schmid, "Review on light management by nanostructures in chalcopyrite solar cells," *Semicond. Sci. Technol.*, vol. 32, 2017, Art. no. 043003.

[28] M. Mostefaoui, H. Mazari, S. Khelifi, A. Bouraiou, and R. Daboua, "Simulation of high efficiency CIGS solar cells with SCAPS-1D software," *Energy Procedia*, vol. 74, pp. 736–744, 2015.

[29] X. Shang *et al.*, "A numerical simulation study of $CuInS_2$ solar cells," *Thin Solid Films*, vol. 550, pp. 649–653, 2014.

[30] M. B. Hosen, A. N. Bahar, M. K. Ali, and M. Asaduzzaman, "Modelling and performance analysis dataset of a CIGS solar cell with ZnS buffer layer," *Data Brief*, vol. 14, pp. 246–250, 2017.

[31] H. Heriche, Z. Rouabah, and N. Bouarissa, "New ultra-thin CIGS structure solar cells using SCAPS simulation program," *Int. J. Hydrogen Energy*, vol. 42, pp. 9524–9532, 2017.

[32] R. Kotipalli *et al.*, "Addressing the impact of rear surface passivation mechanisms on ultra-thin Cu(In,Ga)Se_2 solar cell performances using SCAPS 1-D model," *Sol. Energy*, vol. 157, pp. 603–613, 2017.

[33] D. A. Keszler and J. F. Wager, "Novel materials development for polycrystalline thin-film solar cells: Final subcontract report," Office Sci. Tech. Inf., Oak Ridge, TN, USA, NREL/SR-520-44020, 2008 pp. 1–16.

[34] S. Berge, P. O. Gartland, and B. J. Slagsvold, "Photoelectric work function of a molybdenum single crystal for the (100), (110), (111), (112), (114), and (332) faces," *Surf. Sci.*, vol. 43, pp. 275–292, 1974.

[35] T. Matsukawa *et al.*, "Work function control of Al-Ni alloy for metal gate application, Extended Abstracts of the 2004," in *Proc. Int. Conf. Solid State Devices Mater.*, 2004, vol. 464, pp. 464–465.

[36] J. Krc *et al.*, "Optical confinement in chalcopyrite based solar cells," *Thin Solid Films*, vol. 633, pp. 193–201, 2017.

[37] M. Kovacic *et al.*, "Light management design in ultra-thin chalcopyrite photovoltaic devices by employing optical modelling," *Sol. Energy Mater. Sol. Cells*, vol. 200, 2019, Art. no. 109933.

[38] R. B. M. Girisch, R. P. Mertens, and R. F. De Keersmaecker, "Determination of Si-SiO_2 interface recombination parameters using a gate-controlled point- junction diode under illumination," *IEEE Trans. Electron Devices*, vol. 35, no. 2, pp. 203–222, 1988.

[39] S. Bose *et al.*, "A morphological and electronic study of ultrathin rear passivated Cu(In,Ga)Se_2 solar cells," *Thin Solid Films*, vol. 671, pp. 77–84, 2019.

[40] S. Dongaonkar *et al.*, "Universality of non-Ohmic shunt leakage in thin-film solar cells," *J. Appl. Phys.*, vol. 108, 2010, Art. no. 124509.

[41] S. S. Hegedus and W. N. Shafarman, "Thin-film solar cells: Device measurements and analysis," *Prog. Photovolt., Res. Appl.*, vol. 12, pp. 155–176, 2004.

[42] R. Kotipalli *et al.*, "Investigating the electronic properties of Al_2O_3/Cu(In, Ga)Se_2 interface," *AIP Adv.*, vol. 5, 2015, Art. no. 107101.

[43] R. Kotipalli *et al.*, "Passivation effects of atomic-layer-deposited aluminum oxide," *EPJ Photovolt.*, vol. 4, 2013, Art. no. 45107.

[44] J. Yao *et al.*, "Quantifying losses in open-circuit voltage in solution-processable solar cells," *Phys. Rev. Appl.*, vol. 4, 2015 Art. no. 014020.

[45] G. Sozzi, S. D. Napoli, M. Carrisi, and R. Menozzi, "Assessing the impact of rear point-contact/passivation on CIGS cells with different absorber thickness and grading, in *Proc. IEEE 7th World Conf. Photovolt. Energy Convers.*, 2018, pp. 3044–3047.